Article

Cell Chemical Biology

Dynamics of Proofreading by the *E. coli* Pol III Replicase

Graphical Abstract

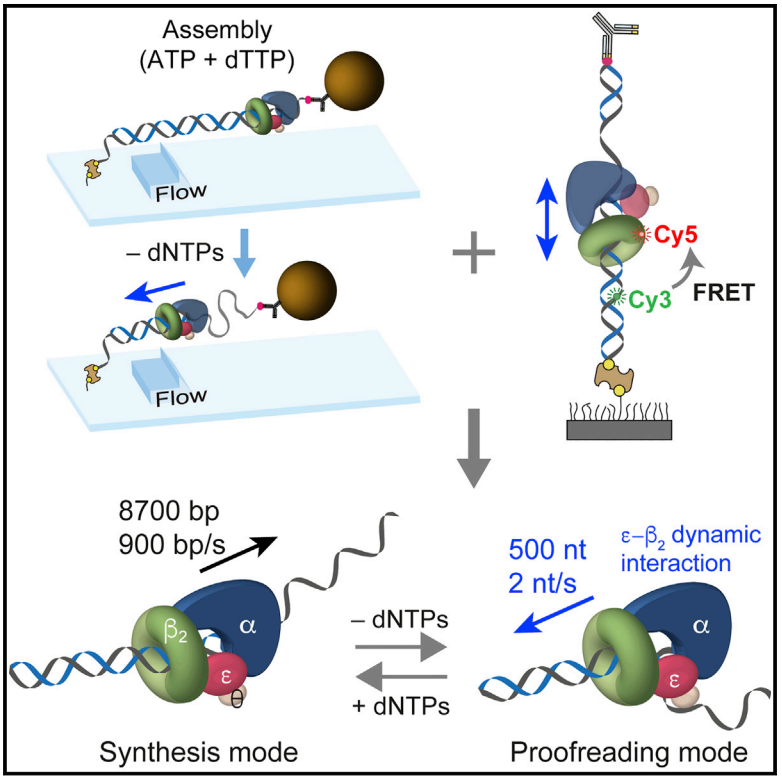

Highlights

- *E. coli* Pol III core-clamp complex is remarkably processive in the absence of dNTPs
- Physical contact between ε and β_2 in both the polymerization and proofreading modes
- Dynamic physical interaction between ε and β_2 during its proofreading activity

Authors

Jonghyun Park, Slobodan Jergic, Yongmoon Jeon, Won-Ki Cho, Ryanggeun Lee, Nicholas E. Dixon, Jong-Bong Lee

Correspondence

nickd@uow.edu.au (N.E.D.), jblee@postech.ac.kr (J.-B.L.)

In Brief

Park et al. revealed real-time dynamic features of the proofreading activity of a chromosomal DNA replicase using single-molecule methods. The dynamic interactions of the subunits provide new insights into the mechanism by which the mismatched primer is delivered from the polymerase site to the exonuclease site, and vice versa.

Park et al., 2018, Cell Chemical Biology *25*, 57–66
January 18, 2018
https://doi.org/10.1016/j.chembiol.2017.09.008

CellPress

Cell Chemical Biology
Article

Dynamics of Proofreading by the *E. coli* Pol III Replicase

Jonghyun Park,[1,4] Slobodan Jergic,[2,4] Yongmoon Jeon,[1] Won-Ki Cho,[1] Ryanggeun Lee,[1] Nicholas E. Dixon,[2,*] and Jong-Bong Lee[1,3,5,*]
[1]Department of Physics, Pohang University of Science & Technology (POSTECH), Pohang 37673, Korea
[2]Centre for Medical and Molecular Bioscience, University of Wollongong & Illawarra Health and Medical Research Institute, Wollongong, NSW 2522, Australia
[3]School of Interdisciplinary Bioscience and Bioengineering, POSTECH, Pohang 37673, Korea
[4]These authors contributed equally
[5]Lead Contact
*Correspondence: nickd@uow.edu.au (N.E.D.), jblee@postech.ac.kr (J.-B.L.)
https://doi.org/10.1016/j.chembiol.2017.09.008

SUMMARY

The αεθ core of *Escherichia coli* DNA polymerase III (Pol III) associates with the β_2 sliding clamp to processively synthesize DNA and remove misincorporated nucleotides. The α subunit is the polymerase while ε is the 3′ to 5′ proofreading exonuclease. In contrast to the polymerase activity of Pol III, dynamic features of proofreading are poorly understood. We used single-molecule assays to determine the excision rate and processivity of the β_2-associated Pol III core, and observed that both properties are enhanced by mutational strengthening of the interaction between ε and β_2. Thus, the ε-β_2 contact is maintained in both the synthesis and proofreading modes. Remarkably, single-molecule real-time fluorescence imaging revealed the dynamics of transfer of primer-template DNA between the polymerase and proofreading sites, showing that it does not involve breaking of the physical interaction between ε and β_2.

INTRODUCTION

Chromosomal replicative DNA polymerases such as the *Escherichia coli* Pol III holoenzyme promote the covalent incorporation of complementary nucleotides to copy a single-stranded DNA (ssDNA) template with a significant intrinsic error rate (10^{-4} to 10^{-5} per nt incorporated). When they incorporate non-complementary nucleotides, replicative polymerases switch between DNA polymerization and proofreading modes to remove the mismatched nucleotides using an associated 3′→5′ exonuclease. This proofreading activity increases the fidelity of DNA synthesis by as much as 1,000-fold (Kunkel, 2004; Johansson and Dixon, 2013). Since most known chromosomal replicases have their proofreading functions embedded in structured domains in the same polypeptide chain as the polymerase (Johansson and Dixon, 2013; Rock et al., 2015), this transition involves a large-scale conformational change that transfers the primer-template between the spatially separated polymerase and exonuclease active sites (Shamoo and Steitz, 1999; Franklin et al., 2001). Detailed kinetic studies of phage T7 and other DNA polymerases with matched and mismatched templates have elucidated the determinants of this transition (Donlin et al., 1991; Capson et al., 1992; Carver et al., 1994). Crystal structures of proofreading domains universally show that 3–4 base pairs (bp) at the mismatched terminus need to be trapped by thermal melting to allow the 3′ mismatched primer terminus to reach the exonuclease active site (Steitz et al., 1987), and this may represent a slow and temperature-dependent step in initiation of exonuclease activity (Brenowitz et al., 1991; Echols and Goodman, 1991).

However, in *E. coli* and many other proteobacteria, the proofreading and polymerase functions of the Pol III replicase reside in separate, interacting subunits (Scheuermann and Echols, 1984), and the transition between the two modes has been proposed to occur by a fundamentally different, but still poorly understood mechanism (Ozawa et al., 2013). The catalytic core of *E. coli* Pol III contains three subunits: α (polymerase), ε (exonuclease), and θ (which binds to ε, but not α) (Lehtinen and Perrino, 2004; McHenry, 2011). When associated with the β_2 sliding clamp, the core alone achieves fast (~350 bp s^{-1}), processive (~1.4 kb) and high-fidelity DNA synthesis (Echols and Goodman, 1991; Tanner et al., 2008). The ring-shaped homodimeric clamp (Kong et al., 1992) encircles the double-stranded (ds) primer-template DNA and stabilizes the core on it in the polymerization mode through both of its symmetry-related hydrophobic protein-binding pockets (Jergic et al., 2013; Toste Rêgo et al., 2013). Proteins that interact with these pockets on the clamp generally do so through short unstructured clamp-binding peptide motifs (CBMs) (Dalrymple et al., 2001; Yin et al., 2013), and the Pol III core contains two of them. One CBM, located at the tip of the fingers domain of α, binds relatively strongly to the clamp (Dohrmann and McHenry, 2005), while the other is a weakly binding CBM (Jergic et al., 2013) at the end of the N-terminal exonuclease domain of ε (Hamdan et al., 2002a). The CBM in ε is in an otherwise unstructured linker region that connects to the C-terminal α-binding region (Jergic et al., 2013; Ozawa et al., 2013). This linker, about 14 residues in length, remains unstructured even in a stabilized αεθ-β_2 complex (Ozawa et al., 2013). Dissociation of the ε CBM from the clamp would thus lead to a situation where εθ would remain flexibly tethered to α.

Use of mutant versions of ε that contained weakened and strengthened CBMs in single-molecule leading strand DNA replication assays showed that strengthening the direct interaction between ε and β_2 enhances both the rate and processivity of DNA synthesis, but not the lifetime of the replicase on DNA, indicating that this interaction is intact in the polymerization mode, but does not directly stabilize the polymerase on the DNA (Jergic et al., 2013). This led us to suggest that the Pol III core must frequently transition between two conformational states termed "open" and "closed" based on X-ray crystal structures (Bailey et al., 2006; Lamers et al., 2006; Wing et al., 2008), where the ε-β contact is broken in the open state, which might be signaled when the polymerase is stalled by incorrect nucleotide incorporation or upon encountering a lesion in the DNA template (Jergic et al., 2013; Ozawa et al., 2013). Intuitively, it seemed likely that replicase stalling by either mechanism would signal similar conformational change in the Pol III core, and release of the ε-β_2 contact would have an obvious role in exposing a hydrophobic cleft in β_2 for entry of a translesion (TLS) polymerase like Pol IV or Pol V (Kath et al., 2014); both of these polymerases have CBMs that interact with the cleft in β_2.

Nevertheless, Toste Rêgo et al. (2013) showed, using an indirect assay, that weakening of the ε-β_2 interaction negatively impacted on the exonuclease activity of the Pol III core, suggesting that this interaction persists in the proofreading as well as the polymerization mode. The exchange between the polymerase and the exonuclease domains is strongly influenced by the presence of dNTPs, as demonstrated for various polymerases by bulk assays (Donlin et al., 1991; Capson et al., 1992; Carver et al., 1994) and for *E. coli* Pol I (Klenow fragment) using single-molecule fluorescence methods (Christian et al., 2009; Santoso et al., 2010; Berezhna and Gill, 2012; Lamichhane et al., 2013). Until now, however, the corresponding dynamics of Pol III in the proofreading mode have not been studied to yield similar insights.

Using single-molecule techniques, we have now visualized the proofreading activity of individual polymerases by reconstituting the *E. coli* Pol III replicase (αεθ and β_2) on primer-template DNAs with the γ clamp loader ($\gamma_3\delta\delta'$) to study the kinetics of the exonuclease activity of the αεθ-β_2 complex in the absence of dNTPs. We first addressed the question of physical contact of ε with the clamp in the proofreading mode using ensemble and tethered bead flow-stretching assays, again with Pol III cores containing ε mutants with modified binding affinity for β_2. Then, single-molecule fluorescence experiments on short DNA templates were used to directly uncover an additional inactive state during the exonuclease activity, corresponding to the transient dissociation of ε from β_2, while α remains tethered to the other protein-binding pocket of the clamp. This inactive (open) state impacts on both the processivity and rate of the exonuclease activity, but does not seem to be involved in transfer of a mismatched primer terminus between the polymerase and exonuclease active sites.

RESULTS

Strand Excision by Single DNA Pol III Core-β_2 Complexes

We designed a multiplexed flow-stretching single-molecule experiment to monitor the transition from ds into ssDNA as a result of exonuclease activity of Pol III. The 3′-biotinylated end of the 45.7-kb dsDNA is attached to a polyethylene glycol (PEG)-passivated coverslip through interaction with neutravidin, and the opposite 5′-digoxigenin (dig) end is linked to a bead (2.8 μm in diameter) functionalized with anti-dig antibody (Figures 1A and 1B). A 2.5 pN hydrodynamic force is applied to the bead, and the immobilized DNA substrate is stretched by laminar flow, such that dsDNA is extended longer than ssDNA (van Oijen et al., 2003). Pol III core (αεθ) and β_2 are recruited by the γ clamp loader ($\gamma_3\delta\delta'$) at the 3′ ssDNA/dsDNA junction comprising a 42-nt ssDNA tail linked to the anti-dig bead. The absence of dNTPs allows observation of the exonuclease activity of αεθ-β_2. We determined the position of the bead in real time to monitor the resulting shortening of the dsDNA substrate (Figure 1B).

To measure the kinetic parameters of strand excision by a single replicase, we preassembled αεθ and β_2 in the presence of the next to be incorporated dNTP (dTTP), which suppresses both the polymerase and exonuclease activities. Exchange to buffers without nucleotides removed the free proteins and dTTP to initiate exonuclease activity (Figure 1C). The number of nucleotides excised was determined based on differences in lengths between ds and ssDNA (Lee et al., 2006). The appearance of a long plateau after 1,000 s in the example trajectory (Figure 1C) indicates the dissociation of Pol III from the DNA substrate. In contrast, in the continuous presence of all three replicase sub-assemblies, but without any dNTPs, we observed continuous DNA shortening (Figures S1A–S1C), indicating that multiple Pol III complexes can reload sequentially to promote strand excision. We also used control experiments to confirm that the shortening observed in Figure 1C requires the activities of both ε and a correctly loaded sliding clamp (Figures S1D–S1G).

In the one case where it has been measured, the processivity of strand excision by the exonuclease activity of Pol III was reported as 44 nt, measured in bulk using a 50-bp substrate (Reems et al., 1991), but this value must be underestimated because the length of the DNA was limited. For the first time, using a long DNA substrate in the absence of dNTPs, we measured a much longer average processivity of the exonuclease activity of individual αεθ-β_2 complexes (471 ± 78 nt; Figure 1D). Surprisingly, the proofreading exonuclease is processive over timescales of several minutes, which contrasts with the much shorter lifetime of the full replisome during leading strand synthesis (Jergic et al., 2013). The average rate of strand excision was measured as 1.6 ± 1.3 nt s^{-1} (Figure 1E), which is much slower than the polymerase rate (~350 bp s^{-1}) in strand extension by the αεθ-β_2 complex (Tanner et al., 2008).

The ε-β Interaction Enhances the Exonuclease Activity of αεθ-β_2

To determine the role of the ε-β contact in the proofreading mode, we examined the exonuclease activities of Pol III complexes containing αεθ cores with two well-characterized mutations in the exonuclease subunit. The mutant ε_Q in which the first residue (Q182) in the conserved CBM (QTSMAF) is replaced by alanine binds much more weakly to β_2 than wild-type ε. Conversely, the mutant ε_L, in which the CBM is changed to QLSLPL, strongly binds to β_2 (Wijffels et al., 2004; Jergic et al.,

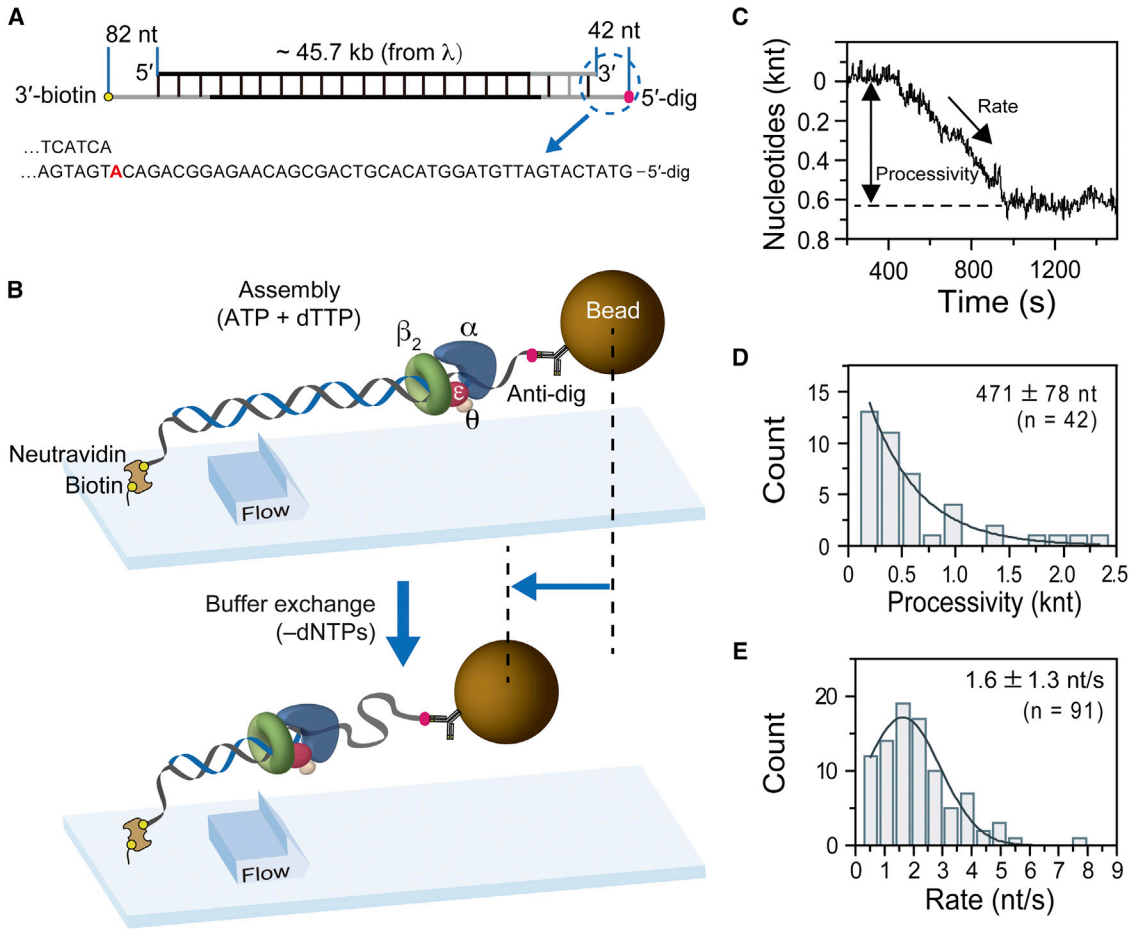

Figure 1. Exonuclease Activity of a Preassembled αεθ-β_2 Complex

(A) Construction of 45.7-kb DNA with a 5′ overhang for measurement of αεθ-β_2 exonuclease activity. In the presence of only dTTP, αεθ-β_2 incorporates only the first nucleotide at the dsDNA/ssDNA junction.

(B) The αεθ-β_2 complex is preloaded by the γ clamp loader onto the junction with dTTP, ATP, and Mg^{2+}. The flow of the reaction buffer, including Mg^{2+} but without nucleotides, initiates the exonuclease activity of the preassembled αεθ-β_2.

(C) A representative trajectory over time was obtained from the length change between dsDNA and ssDNA, enabling determination of the exonuclease rate and processivity of individual αεθ-β_2 complexes.

(D and E) Histograms of the processivity (n = 42, the number of molecules) and the rate (n = 91, the number of rates measured in 42 molecules), fit to a single exponential decay function (processivity) or single Gaussian distribution (rate). Errors are SEM from fitting errors (processivity) and SD (rate) of the distributions. [β_2] = 30 nM, [$\gamma_3\delta\delta'$] = 15 nM, [αεθ] = 30 nM, [dTTP] = 100 μM.

2013). Use of the ε_L core complex enhances the rate and processivity of helicase-coupled leading strand DNA synthesis, while use of the ε_Q core decreases both parameters (Jergic et al., 2013). We used cores containing these mutant ε subunits to define the significance of the ε-β interaction in the proofreading mode.

We first analyzed the exonuclease activity of αε_Lθ-β_2, αεθ-β_2, and αε_Qθ-β_2 in an ensemble assay with singly nicked 7.3-kb circular DNA (Figures 2A and S2A). Among them, αε_Lθ-β_2 was the most active in DNA degradation, while αε_Qθ-β_2 appeared to have very little activity. Figure 2B shows a representative time trajectory of 3′→5′ exonuclease activity of a single preassembled ε_L mutant replicase using the flow-stretching assay. The exonuclease events mediated by αε_Lθ-β_2 were observed 50% more frequently than those by αεθ-β_2, and shortening events mediated by the αε_Qθ-β_2 complex were rarely observed (2%), which is consistent with the result in the bulk measurement (Figures 2A and 2C). Taken together, these data indicate that the ε-β interaction plays a role in loading or stabilization of the replicase on the primed template DNA in the presence of the incoming dNTP.

The presence of free proteins (αε_Qθ or αε_Lθ, β, and γ clamp loader) in solution dramatically increased the yield of exonuclease events (Figures S2B and S2C). These results might indicate that a single αε_Qθ-β_2 removes less than 120 nt (the spatial resolution of the flow-stretching assay) before it dissociates. The processivity (810 ± 110 nt) and rate (3.2 ± 1.8 nt s^{-1}) of preassembled αε_Lθ-β_2 were higher than those of αεθ-β_2 (Figures 2D and 2E; $p < 0.01$). Thus, these data clearly show that direct contact between ε and β stimulates the proofreading as well as polymerase activity of αεθ-β_2, and that the replicase is therefore in the closed state during both processes.

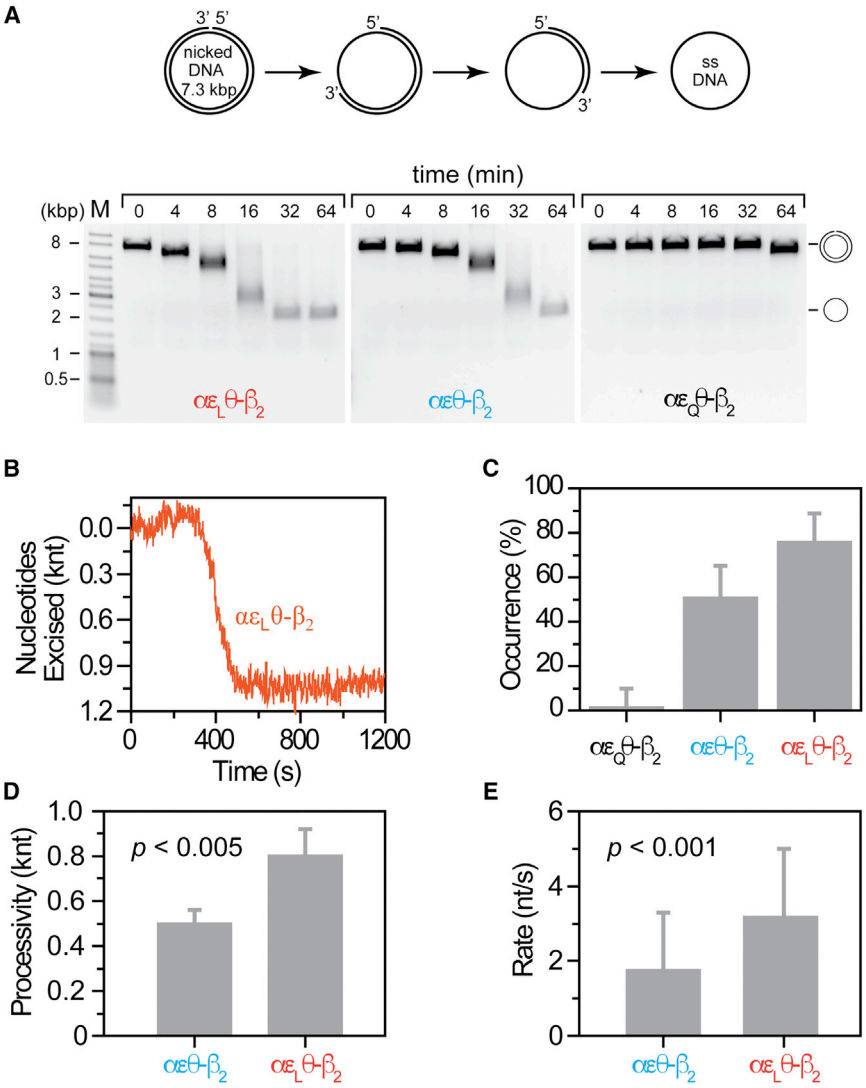

Figure 2. The Exonuclease Activity of Cores Containing ε Variants

(A) A primer degradation ensemble assay by $\alpha\varepsilon\theta$-β_2, $\alpha\varepsilon_L\theta$-$\beta_2$, $\alpha\varepsilon_Q\theta$-$\beta_2$ (ε_L, stronger binding to β_2; ε_Q, weaker binding to β_2). [β_2] = 200 nM, [$\gamma_3\delta\delta'$] = 50 nM, [$\alpha\varepsilon\theta$] = [$\alpha\varepsilon_L\theta$] = [$\alpha\varepsilon_Q\theta$] = 100 nM, [ATP] = 1 mM.

(B) A representative time trajectory of $\alpha\varepsilon_L\theta$-$\beta_2$ (orange).

(C) The ratio of the exonuclease events to the number of DNA substrates observed: $\alpha\varepsilon_Q\theta$-$\beta_2$ (2% ± 7%), $\alpha\varepsilon\theta$-β_2 (51% ± 14%), and $\alpha\varepsilon_L\theta$-$\beta_2$ (76% ± 12%). The error bars indicate SD derived from multiple trajectories in three independent experiments.

(D) The exonucleolytic processivities of $\alpha\varepsilon\theta$-β_2 (470 ± 80 nt; n = 42) and $\alpha\varepsilon_L\theta$-$\beta_2$ (810 ± 110 nt; n = 130) were determined as exponential fits to the processivity distribution [p value (p) = 2.7×10^{-3}]. The error bars indicate fitting errors (mean ± SEM).

(E) The rates of $\alpha\varepsilon\theta$-β_2 (1.6 ± 1.3 nt s^{-1}; n = 91) and $\alpha\varepsilon_L\theta$-$\beta_2$ (3.2 ± 1.8 nt s^{-1}; n = 186) were determined after fitting a Gaussian distribution (p = 1.9×10^{-12}). The error bars indicate SD. In (C)–(E): [β_2] = 30 nM, [$\gamma_3\delta\delta'$] = 15 nM, [$\alpha\varepsilon\theta$] = [$\alpha\varepsilon_L\theta$] = [$\alpha\varepsilon_Q\theta$] = 30 nM, [dTTP] = 100 μM.

Polymerase Exchange in the Proofreading Mode

Transient disruption of either the α-β or ε-β interaction during proofreading could enable binding of a new polymerase to the vacant site on β_2, facilitating its access to the 3′-primer terminus by displacement of the previously loaded $\alpha\varepsilon\theta$ core, a dynamic exchange process similar to those demonstrated with the phage T7 replisome (Hamdan et al., 2007; Johnson et al., 2007; Geertsema et al., 2014). To test exchange among polymerase cores, we introduced $\alpha\varepsilon_{DEAD}\theta$ without dNTPs in a sample chamber in which $\alpha\varepsilon\theta$-β_2 or $\alpha\varepsilon_L\theta$-$\beta_2$ had been preloaded onto the DNA substrate in the presence of dTTP (Figure 3A); ε_{DEAD} is the D12A/E14A mutant of ε, which has no residual exonuclease activity (Fijalkowska and Schaaper, 1996) (Figure S1G), but sustains DNA synthesis (Jergic et al., 2013). We anticipated one of three outcomes: if dynamic exchange occurred frequently, the observed yield of exonuclease trajectories would approach zero within the spatial resolution of our assay, while if exchange occurred less frequently, the processivity of the Pol III cores would appear to be reduced. Thirdly, if exchange required complete dissociation of the active cores after their dwell time on DNA, processivity should be unaffected. In fact, the yield of exonuclease events was reduced to ~20% (from ~50%) with preloaded $\alpha\varepsilon\theta$-β_2 and to ~70% (from ~80%) with preloaded $\alpha\varepsilon_L\theta$-$\beta_2$ (Figures 2C and 3B; the inset in Figure 3B shows representative trajectories of individual molecules). Moreover, the average processivities among trajectories of multiple molecules were in each case reduced by a factor of ~2 (Figure 3C; $p < 0.01$). Note, however, that the reduction is likely to be larger than this because we were unable to observe the shortest events. Thus, while dynamic exchange of Pol III cores can be observed during proofreading, the core-β_2 complexes seem to be rather resilient to it when in the proofreading mode.

We also observed increased exonuclease activity when $\alpha\varepsilon_L\theta$ was added in the chamber after $\alpha\varepsilon\theta$-β_2 had been preloaded on DNA (Figure 3D). The processivity and rate were identical to those of $\alpha\varepsilon_L\theta$-$\beta_2$ (Figures 2E and 3D). Furthermore, an abrupt rate change was clearly observed, confirming exchange between $\alpha\varepsilon\theta$ and $\alpha\varepsilon_L\theta$ (Figure 3E). Taken together, these observations indicate that dynamic exchange of polymerase cores can occur before their complete dissociation from the DNA substrate, but that it occurs infrequently. This is consistent with both CBMs being in contact with the clamp for the majority of the time the replicase spends in the proofreading mode.

Single-molecule FRET Informs on the Dynamics of $\alpha\varepsilon\theta$-β_2

To exploit single-molecule fluorescence resonance energy transfer (smFRET) to access detailed kinetic features, we first

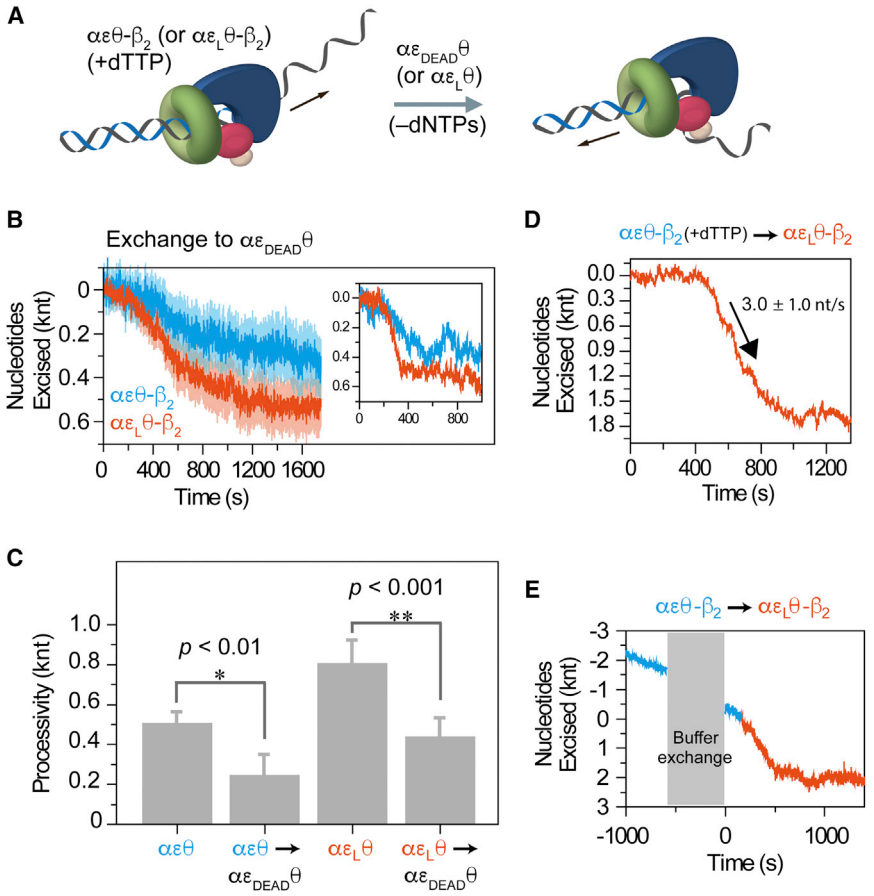

Figure 3. Polymerase Exchange

(A) $\alpha\varepsilon\theta$-β_2 (or $\alpha\varepsilon_L\theta$-$\beta_2$) was preassembled with dTTP, and subsequently $\alpha\varepsilon_{DEAD}\theta$ (or $\alpha\varepsilon_L\theta$) was introduced without any nucleotides. Note that β_2 and $\gamma_3\delta\delta'$ are not present during exchange, so trajectories become flat when the core-β_2 contact is irretrievably lost. [β_2] = 30 nM, [$\gamma_3\delta\delta'$] = 15 nM, [$\alpha\varepsilon\theta$] = [$\alpha\varepsilon_{DEAD}\theta$] = [$\alpha\varepsilon_L\theta$] = 30 nM, [dTTP] = 100 μM.

(B) $\alpha\varepsilon\theta$-β_2 (or $\alpha\varepsilon_L\theta$-$\beta_2$) was preloaded on DNA with dTTP and then $\alpha\varepsilon_{DEAD}\theta$ was infused without dNTPs. The processivities were measured to be 250 ± 100 nt (n = 18) for $\alpha\varepsilon\theta$-β_2 → $\alpha\varepsilon_{DEAD}\theta$ and 440 ± 90 nt (n = 28) for $\alpha\varepsilon_L\theta$-$\beta_2$ → $\alpha\varepsilon_{DEAD}\theta$, which were significantly less than those of $\alpha\varepsilon\theta$-β_2 or $\alpha\varepsilon_L\theta$-$\beta_2$ (Figure 2). The errors indicate fitting errors (SEM). Inset: representative trajectories of $\alpha\varepsilon\theta$-β_2 (light blue) and $\alpha\varepsilon_L\theta$-$\beta_2$ (orange). The yield of exonuclease events was also reduced to 17% (23/139) and 70% (29/42) for $\alpha\varepsilon\theta$-β_2 → $\alpha\varepsilon_{DEAD}\theta$ and $\alpha\varepsilon_L\theta$-$\beta_2$ → $\alpha\varepsilon_{DEAD}\theta$, respectively.

(C) The exonuclease processivity obtained from $\alpha\varepsilon\theta$ → $\alpha\varepsilon_{DEAD}\theta$ (250 ± 100 nt; n = 18) compared with $\alpha\varepsilon\theta$-β_2 (~470 nt) ($p = 9.9 \times 10^{-3}$) and $\alpha\varepsilon_L\theta$ → $\alpha\varepsilon_{DEAD}\theta$ (440 ± 90 nt; n = 28) to $\alpha\varepsilon_L\theta$-$\beta_2$ (~810 nt) ($p = 6.1 \times 10^{-6}$). The error bars indicate fitting errors (mean ± SEM).

(D) When $\alpha\varepsilon\theta$ in preassembled $\alpha\varepsilon\theta$-β_2 was exchanged to $\alpha\varepsilon_L\theta$ without dNTPs, the exonuclease activity stopped after 1,650 nt were excised. The processivity and rate (mean ± SEM, from fitting) appeared to be 830 ± 110 nt (n = 51) and 3.0 ± 1.0 nt/s (n = 61), respectively.

(E) $\alpha\varepsilon_L\theta$ was introduced in the sample chamber at 0 s, where $\alpha\varepsilon\theta$-β_2 was already loaded. The slope seems to have changed in a steeper direction at 200 s.

constructed an 85-bp DNA duplex with a 12-nt gap of ssDNA in the middle (Figure 4A). The 5′-biotinylated end of the DNA substrate was immobilized on a PEG/PEG-biotin passivated surface via a biotin-streptavidin interaction and the 3′-dig end was blocked to prevent the rapid dissociation of β_2, as described previously (Cho et al., 2014). We detected FRET signals from the donor Cy3 attached to the 28th nucleotide upstream of the dsDNA/ssDNA junction and the acceptor Cy5 conjugated to one of the Cys333 residues of β_2 (Cho et al., 2014). After loading the clamp onto the duplex by incubating it with the γ clamp loader and ATP, we infused $\alpha\varepsilon\theta$ with dNTPs into the sample chamber at 5 s. The FRET efficiency of 0.52 ± 0.12 decreased over a few seconds to 0.16 ± 0.08 (Figure 4B). The intermediate FRET of the first state resulted from preloaded Cy5-β_2 rapidly diffusing on the Cy3-DNA (Cho et al., 2014). As $\alpha\varepsilon\theta$-β_2 promoted nucleotide incorporation, Cy5-β_2 became more distant from Cy3, thereby decreasing the FRET efficiency.

In contrast, when $\alpha\varepsilon\theta$ was added without dNTPs, the FRET value initially increased from ~0.5 to 0.67 ± 0.12 (Figure 4C). Thus, $\alpha\varepsilon\theta$-Cy5-β_2 moved closer to Cy3 while removing nucleotides upstream of the dsDNA/ssDNA junction, as anticipated based on the previous observation (Figure 1). In this experimental condition, the space of 15 bp between the 5′-biotin attached to the surface and the Cy3 on DNA is insufficient to allow the $\alpha\varepsilon\theta$-Cy5-β_2 complex to excise the Cy3-nucleotide, since the distance from the back side of β_2 to the primer terminus is ~25 bp (Fernandez-Leiro et al., 2015). Therefore, the $\alpha\varepsilon\theta$-Cy5-β_2 complex is likely to stop in front of Cy3.

We purposely placed a single thymidine in the ssDNA gap to examine how the kinetics of $\alpha\varepsilon\theta$-Cy5-β_2 responds when the complex cannot accomplish nucleotide incorporation in the absence of dATP. As shown in Figure 4D, the absence of dATP among dNTPs also decreased the FRET efficiency (to 0.27 ± 0.11), but the FRET value of the final state was significantly higher than that in the presence of all four dNTPs. The result implies that the $\alpha\varepsilon\theta$-Cy5-β_2 complex stalled at the unique thymidine site in the gap, and did not generate a mismatch to bypass. This is consistent with the stable preassembly of the $\alpha\varepsilon\theta$-β_2 complex in the presence of only dTTP in the flow-stretching experiments (Figure 1).

Proofreading by $\alpha\varepsilon\theta$-β_2 Is Inhibited When the ε-β Interaction Is Disrupted

In the previous section, we confirmed that the $\alpha\varepsilon\theta$-β_2 complex, but not $\alpha\varepsilon\theta$ alone (at the low concentration used), displayed its catalytic reactions of DNA synthesis and exonuclease activity. To better resolve its exonuclease activity at higher spatial resolution, both donor (Cy3) and acceptor (Cy5) were attached at a 23-bp (~7.8 nm) distance on the duplex (Figure 5A), which is expected to generate a FRET value of ~0.2 (Figure S3A). In the cryoelectron microscopy (cryo-EM) structure of $\alpha\varepsilon\beta_2\tau$ on primer-template DNA, this places Cy5 in a widely exposed

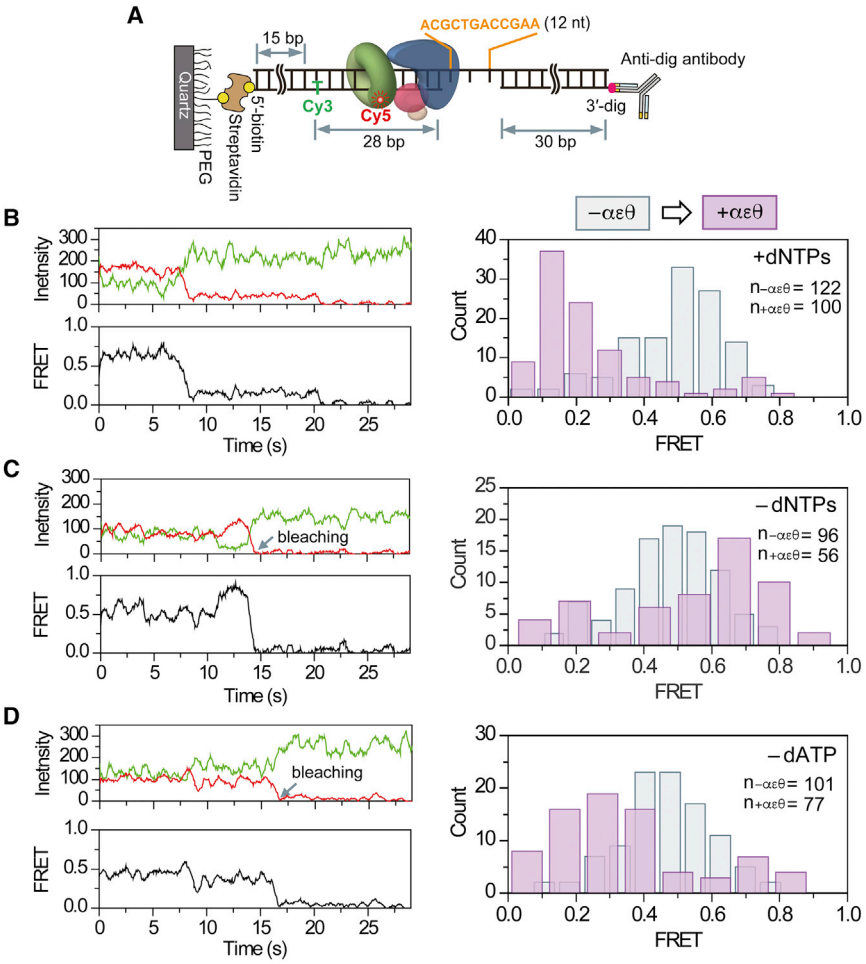

Figure 4. smFRET between Cy3 on a DNA Substrate and Cy5-Labeled β_2 in an $\alpha\varepsilon\theta$-β_2 Complex

(A) A DNA substrate including a 12-nt gap and a Cy3 donor. The FRET efficiency between Cy3 and loaded and freely diffusing (Cho et al., 2014) Cy5-β_2 was 0.49 ± 0.14 in the absence of $\alpha\varepsilon\theta$. For clamp loading, [β_2] = 30 nM, [$\gamma_3\delta\delta'$] = 15 nM. Representative traces of emission intensities and FRET efficiency and histograms of FRET efficiency before and after the infusion of 30 nM $\alpha\varepsilon\theta$ at 5 s, with:

(B) +dNTPs (100 μM each);

(C) –dNTPs;

(D) +dGTP, +dTTP, +dCTP (100 μM each), but –dATP. The FRET values showed transitions from ~0.5 to 0.16 ± 0.08 (+dNTPs), 0.67 ± 0.12 (–dNTPs), and 0.27 ± 0.11 (–dATP). All errors in the FRET efficiency indicate SD. The arrow in each panel indicates a photo-bleaching step.

position between the PHP and fingers domains of α (Fernandez-Leiro et al., 2015). The unlabeled preloaded β_2 clamps did not affect the FRET of Cy3-Cy5 on the duplex (Figure S3B). After replacing the β_2 and γ clamp loader solution in the sample chamber with just $\alpha\varepsilon\theta$ (but without dNTPs) at 5 s into the observation period, we observed a gradual increase in the FRET efficiency from 0.2 to 0.5 due to the shortening transition of dsDNA into ssDNA between the Cy3-Cy5 FRET pair as a result of exonuclease activity (Figures 5B and S3C); the FRET change was not observed with $\alpha\varepsilon_{DEAD}\theta$ (Figure S3D). We also confirmed that there was no FRET change caused by $\alpha\varepsilon\theta$ alone in the absence of β_2 and that the Cy5 near the ssDNA/dsDNA junction did not obstruct the diffusion of a β_2 clamp or the exonuclease activity of the $\alpha\varepsilon\theta$-β_2 complex. As expected, because the $\alpha\varepsilon\theta$-β_2 complex incorporates nucleotides, the presence of dNTPs resulted in decreased FRET efficiency due to the lengthening of DNA in an alternate reporter DNA construct (Figures S3E–S3H), while in the absence of dNTPs, FRET efficiency increased modestly over time due to the exonuclease activity. Together these results indicate that the exonuclease activity of the $\alpha\varepsilon\theta$-β_2 complex removes nucleotides upstream of the ssDNA/dsDNA junction, as expected.

Remarkably, however, with the primer-template in Figure 5A, we observed short-lived pauses during the increase (exonuclease activity) in many FRET trajectories, as shown in Figure 5B. The pauses were identified objectively by applying a step-finding algorithm to the FRET transition region of the trajectory (Kalafut and Visscher, 2008), and occurred in ~20% of trajectories for $\alpha\varepsilon_Q\theta$-$\beta_2$, increasing to 60%–70% for the wild-type and ε_L cores. The exonuclease activity of $\alpha\varepsilon\theta$-β_2 showed a broad distribution of FRET values corresponding to the pauses (Figure S4A), showing that Pol III stalling occurs at random positions on the substrate. Critically, the duration of the FRET pauses (τ_{pause}) was observed to depend inversely on the strength of the ε-β_2 interaction: pausing of $\alpha\varepsilon_Q\theta$-$\beta_2$ (30.4 ± 1.5 s) was much longer than of $\alpha\varepsilon\theta$-β_2 (3.7 ± 0.4 s), while that of $\alpha\varepsilon_L\theta$-$\beta_2$ (2.5 ± 0.2 s) was 30% shorter (p = 0.017; Figures 5C and S4C). This observation strongly suggests that disruption of the ε-β interaction occurs during the pauses, and stalls exonuclease activity.

With $\alpha\varepsilon_Q\theta$-$\beta_2$, the final FRET of each trajectory reached ~0.4 in the total time window (~150 s); this was lower than the final FRET efficiency (~0.5) for $\alpha\varepsilon\theta$-β_2 and $\alpha\varepsilon_L\theta$-$\beta_2$ (Figure S4B). This observation implies impaired exonuclease activity of $\alpha\varepsilon_Q\theta$-$\beta_2$, consistent with the results of the flow-stretching assay where exonuclease events were rarely observed (Figures 2A and 2C). Most of the exonuclease events we have observed might be stopped at the first pauses, which probably explains the infrequent pausing of $\alpha\varepsilon_Q\theta$-$\beta_2$. Therefore, the transient pauses during exonuclease activity result from the stochastically fluctuating interaction between ε and β_2, where the interaction is absent during pauses; ε is known to be highly mobile in the context of the $\alpha\varepsilon\theta$-β_2 complex (Ozawa et al., 2013).

Unexpectedly, the Cy3 signal abruptly increased soon after injection of $\alpha\varepsilon\theta$ into the sample chamber to interact with β_2 diffusing on DNA (at 5 s in the sample trace in Figure 5B).

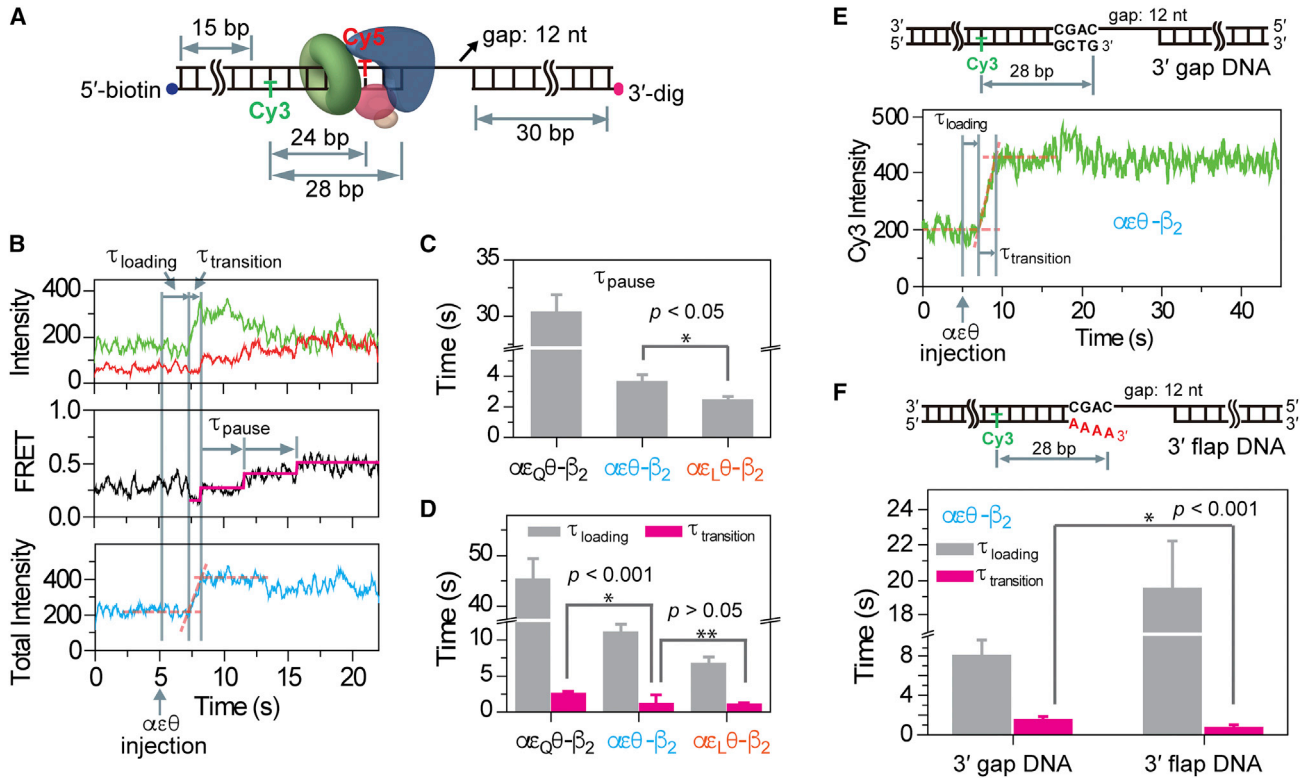

Figure 5. The Intermediate State Detected during the Exonuclease Activity of αεθ-β_2

(A) A DNA substrate including a Cy3-Cy5 pair and a 12-nt gap. The duplex DNA between Cy3 and Cy5 is degraded and converted to ssDNA by the replicase, resulting in shortening of the gap and increased FRET efficiency. [β_2] = 30 nM, [$\gamma_3\delta\delta'$] = 15 nM, [αεθ] = [$\alpha\varepsilon_Q\theta$] = [$\alpha\varepsilon_L\theta$] = 30 nM.

(B) Representative trajectories of the emission intensity, the resulting FRET efficiency, and the total intensity of Cy3 and Cy5. Emission of Cy3 was enhanced right after the proteins were introduced ($\tau_{loading}$) and transient pauses (τ_{pause}) were observed during the FRET increase.

(C) τ_{pause} of $\alpha\varepsilon_Q\theta$-$\beta_2$ (30.4 ± 1.5 s, n = 46), αεθ-β_2 (3.7 ± 0.4 s, n = 82), and $\alpha\varepsilon_L\theta$-$\beta_2$ (2.5 ± 0.2 s, n = 67). All error bars in (C, D, F) indicate fitting errors (mean ± SEM). *p = 1.7 × 10^{-2} for τ_{pause} of αεθ-β_2 and $\alpha\varepsilon_L\theta$-$\beta_2$.

(D) $\alpha\varepsilon_Q\theta$-$\beta_2$: $\tau_{loading}$ = 45.5 ± 3.9 s (n = 112), $\tau_{transition}$ = 2.7 ± 0.2 s (n = 113); αεθ-β_2: $\tau_{loading}$ = 11.2 ± 1.0 s (n = 84), $\tau_{transition}$ = 1.3 ± 0.2 s (n = 73); $\alpha\varepsilon_L\theta$-$\beta_2$: $\tau_{loading}$ = 6.8 ± 0.8 s (n = 128), $\tau_{transition}$ = 1.2 ± 0.1 s (n = 117). *p = 1.3 × 10^{-8} for $\tau_{transition}$ of $\alpha\varepsilon_Q\theta$-$\beta_2$ and αεθ-β_2, **p = 0.07 for $\tau_{transition}$ of αεθ-β_2 and $\alpha\varepsilon_L\theta$-$\beta_2$.

(E) A representative smPIFE trajectory on the DNA template used in Figure 4 (3′ gap DNA) in the presence of αεθ-β_2.

(F) A 3′ flap DNA template with four mismatched nucleotides. The loading and transition times measured by smPIFE in the presence of αεθ-β_2. 3′ gap DNA: $\tau_{loading}$ = 8.1 ± 1.5 s (n = 100), $\tau_{transition}$ = 1.6 ± 0.2 s (n = 98); 3′ flap DNA: $\tau_{loading}$ = 19.5 ± 2.6 s (n = 114), $\tau_{transition}$ = 0.8 ± 0.1 s (n = 114). *p = 1.5 × 10^{-7} for $\tau_{transition}$.

The time ($\tau_{loading}$) from the injection of αεθ to the increase in Cy3 fluorescence intensity was inversely dependent on the concentration of αεθ (Figures S5A–S5E) and was longer for a weaker interaction between ε and β_2 (Figures 5D and S4D), so it corresponds to loading of the replicase complex, associated with β_2 at the primer terminus. We can exclude a dead time until the infusion reached the observation volume from the loading time due to the quick injection of αεθ into the flow chamber. The time-dependent fluorescence enhancement ($\tau_{transition}$) can therefore be attributed to an event following loading of αεθ (Figure 5D). Since we did not observe the fluorescence increase for αεθ-β_2 in the presence of dNTPs (the polymerization mode), and it occurs prior to the onset of exonuclease activity, it must result from the αεθ-β_2 complex transitioning to the proofreading mode at the dsDNA/ssDNA junction. However, curiously we have observed a short time lag (τ_{lag} = 2.5 ± 0.3 s) after the fluorescence enhancement but before initiation of exonuclease activity (Figure S5A). Neither $\tau_{transition}$ nor τ_{lag} was affected by strengthening of the ε-β interaction by use of ε_L compared with wild-type ε, indicating that the ε-β contact must remain intact during these steps (Figures 5D, S5C, and S5E). Nevertheless, both time constants were significantly longer for $\alpha\varepsilon_Q\theta$-$\beta_2$, suggesting difficulty in correctly positioning ε in the near-complete absence (Jergic et al., 2013) of the ε-β contact, consistent with the structural flexibility of the core-clamp complex described by Ozawa et al. (2013).

To simplify observation of protein induced Cy3 fluorescence enhancement (single-molecule protein induced fluorescence enhancement [smPIFE]; Hwang et al., 2011) by the αεθ-β_2 complex, we used an identical (3′ gap DNA) template, but without Cy5 (Figure 5E). The Cy3 emission signal increased in the presence of αεθ with preloaded β_2, but without dNTP (Figure 5E). The loading and transition times (Figure 5F) were nearly identical to those in Figure 5D. Remarkably, use of a 4-nt unpaired primer-template DNA at the junction (3′ flap DNA) resulted in a 2.5-fold increase of the loading time ($\tau_{loading}$ = 19.5 ± 2.6 s; Figures 5F and S5F), which shows that the 3′ ssDNA flap inhibits the initial

complex formation of αεθ with the preloaded β_2. In contrast, the unpaired ssDNA at the junction facilitates transition to the proofreading mode ($\tau_{transition}$ = 0.8 ± 0.1 s; Figures 5F and S5G), since the 3′→5′ exonuclease activity of the αεθ-β_2 complex favors the pre-melted 3′ ssDNA (Park and O'Donnell, 2009). Taken together with the observation of the presence of PIFE in the proofreading mode, the results are consistent with the notion that the exonuclease activity is normally initiated a few seconds after complex formation, denoted as $\tau_{waiting}$ (= $\tau_{transition}$ + τ_{lag}; Figure S5A). This waiting time did not significantly depend on the ε-β binding strength or the concentration of αεθ (Figures 5D, S4E, S5D, and S5E), and the significant decrease of $\tau_{transition}$ at the unpaired primer-template DNA reflects shortening of the time normally required for melting of the dsDNA/ssDNA junction to access the active site of ε (Hamdan et al., 2002a).

We conclude that transition from polymerization to proofreading modes occurs without major conformational rearrangements that would result from opening of the ε-β interaction. We also suspect that a time lag (~2.5 s) might indicate the existence of an intermediate state during transition to the conformation of the exonuclease before initiation of nucleotide excision.

DISCUSSION

We have been successful for the first time in visualizing individual DNA Pol III molecules in the proofreading mode. The αεθ-β_2 complex was reconstituted at a dsDNA/ssDNA junction in the presence of a single dNTP, preventing both its processive proofreading and polymerization activities. Indeed, smFRET experiments revealed that when an αεθ-β_2 complex could not incorporate a nucleotide into the template it was indefinitely stalled, probably due to futile cycles of nucleotide misincorporation and proofreading (Figure 4). Nevertheless, the 3′→5′ exonuclease activity of preassembled αεθ-β_2 initiated after removing dNTPs from solution. The average exonuclease rate (~2 nt s^{-1}) of single replicase complexes is 200-fold slower than the polymerization rate (Tanner et al., 2008), which is consistent with ensemble measurements: the rate of the exonuclease alone is dramatically reduced ($k < 0.04\ s^{-1}$) for duplex DNA versus ssDNA ($k > 200\ s^{-1}$) (Reems et al., 1991; Miller and Perrino, 1996), and showed a strong temperature dependence (Brenowitz et al., 1991). These results imply that a slow step of the exonuclease reaction is the thermal melting of the dsDNA/ssDNA junction to allow the terminus of the mismatched primer to reach and become stabilized at the proofreading active site, which explains the decrease of $\tau_{transition}$ on the 3′ flap DNA (Figure 5F). In previous ensemble experiments, the processivity of Pol III in the exonuclease mode was shown to be > 44 nt (Reems et al., 1991). This single-molecule study clearly shows that a single αεθ-β_2 complex is remarkably more processive (~500 nt) and stable over several minutes in the proofreading mode. In fact, we have not observed significant nucleotide excision by αεθ in the absence of β_2 even in smFRET experiments with nanometer spatial resolution. The results demonstrate that a loaded β_2 clamp stabilizes αεθ through its direct interaction with ε during exonuclease activity, as shown previously in the polymerization mode (Jergic et al., 2013).

The dramatic decrease of the exonuclease activity of $\alpha\varepsilon_Q\theta$, in which ε weakly interacts with β_2, is also strong evidence that the ε-β contact in αεθ-β_2 is required for both proofreading and polymerization modes (Figure 2). These results, therefore, extend our previous model (Jergic et al., 2013) that the overall polymerization rate is dependent on an equilibrium between open and closed states modulated by the strength of the ε-β interaction to include a similar mechanism affecting the rate in the proofreading mode as well. That the ε-β interaction is intact in the proofreading mode is consistent with the recent cryo-EM structure of a Pol III core-β_2 complex in this mode (Fernandez-Leiro et al., 2017).

We initially hypothesized that in the absence of dNTPs, bursts of faster exonuclease activity in the closed state are interspersed by futile attempts to transfer back to the polymerization mode via an intermediate, more open, state in which the ε-β interaction is broken; i.e., the ε-β interaction is intact in both replicase modes, but is disrupted during transition between them. We therefore used smFRET and smPIFE to explore how a primer may be transferred from the polymerase (α) to the exonuclease active site (ε). We were able to observe this transition after initial loading of αεθ on β_2 at the primer terminus (Figures 5B and 5E), but the time constant describing it ($\tau_{transition}$) was independent of the strength of the ε-β interaction (Figure 5D), implying that primer transfer must also occur in a closed state of the complex.

Nevertheless, we did observe pausing events in time trajectories of the exonuclease activity in both the flow-stretching assay (Figures S2D–S2F) and smFRET experiments (Figures 5B, 5C, S4A, and S4C); such pauses were not observable in the polymerization mode (Tanner et al., 2008; Jergic et al., 2013). The pause frequency in the flow-stretching assay was measured to be lower than that in the smFRET experiments due to much poorer time and spatial resolution. The increase of the dwell time of the pauses in smFRET experiments, when the ε-β interaction is weaker (Figures 5C and S4C), excludes that pausing results from base-pair melting at the ssDNA/dsDNA junction. Although it has been previously reported that *E. coli* Pol I (Santoso et al., 2010) and phage ϕ29 polymerase (Ibarra et al., 2009) also showed stalling during exonuclease activity, attributed to the transfer of mismatched primers between the two active sites, we have no evidence of this with Pol III.

Thus, we suggest that the αεθ-β_2 pausing results from breaking of the physical interaction between ε and β during proofreading, but is not associated normally with the bidirectional transfer of the mismatched primer between the α and ε catalytic sites. The highly mobile ε is expected to induce a large conformational change of αεθ-β_2 during the pausing event (Ozawa et al., 2013). The resulting conformation dissociates ε from β_2, for which the affinity is low (K_D ~200 μM) (Jergic et al., 2013), while α remains bound to the other site in β_2. The open structural state of αεθ-β_2 is also likely reflected in the dynamic polymerase core exchange observed in the proofreading mode (Figure 3), presumably involving release of the ε CBM from β_2 for the entry of other β-binding proteins, while the α CBM initially remains tethered to the other protein-binding pocket of β_2 (Sutton, 2010; Kath et al., 2014; Lewis et al., 2017).

The CBM in *E. coli* ε has apparently evolved to be a rather weak one to provide a fine balance between the need to ensure high rate and processivity of the replicase, while enabling detachment of ε from β_2 to enable both polymerase exchange and entry of a TLS polymerase when a lesion is encountered (Kath et al., 2014). Defects in proofreading can be detected *in vivo* as an elevated

mutation rate, i.e., a mutator phenotype. Modulation of the fine balance in the ε_Q and ε_L mutant *dnaQ* genes might be predicted in both cases to produce a mutator phenotype *in vivo*, as recently observed by Whatley and Kreuzer (2015); the ε_Q mutant would be less able to establish the ε-β contact required for proofreading, while ε_L would interfere with entry of other β_2-binding proteins into the replisome when required for DNA repair and other normal processes.

SIGNIFICANCE

For chromosomal DNA replication in *E. coli*, the replicative polymerase III (Pol III) core (α, ε, and θ complex) physically interacts with a sliding DNA clamp (β_2). Using a novel single-molecule flow-stretching technique, complemented by single-molecule FRET experiments, we found that *E. coli* Pol III core-β_2 complex is remarkably processive in the proofreading mode, and the physical interaction between the exonuclease (ε) and β_2 domains is "dynamic" during its proofreading activity. We show that ε interacts directly with β_2 in both the polymerization and proofreading modes. Remarkably, single-molecule real-time fluorescence imaging revealed the dynamics of transfer of primer-template DNA between the polymerase and proofreading sites, showing that it does not involve breaking of the physical interaction between ε and β_2.

STAR★METHODS

Detailed methods are provided in the online version of this paper and include the following:

- KEY RESOURCES TABLE
- CONTACT FOR REAGENT AND RESOURCE SHARING
- EXPERIMENTAL MODEL AND SUBJECT DETAILS
  - Cell Lines and Culture Conditions
- METHOD DETAILS
  - Replication Proteins
  - 45.7 kb DNA for Flow-Stretching Assay
  - Short DNAs for FRET and smPIFE Assays
  - 2.8 μm Super-Paramagnetic Beads
  - Flow-Stretching Assays
  - Ensemble DNA Replication Assays
  - Single-Molecule Fluorescence Imaging
- QUANTIFICATION AND STATISTICAL ANALYSIS
  - Flow-Stretching Assays
  - Single-Molecule Fluorescence Imaging
- DATA AND SOFTWARE AVAILABILITY

SUPPLEMENTAL INFORMATION

Supplemental Information includes five figures and can be found with this article online at https://doi.org/10.1016/j.chembiol.2017.09.008.

AUTHOR CONTRIBUTIONS

Conceptualization, J.P., S.J., N.E.D., and J.-B.L.; Investigation, J.P., S.J., Y.J., W.-K.C., and R.L.; Writing – Original Draft, J.P., S.J., N.E.D., and J.-B.L.; Writing – Review & Editing, J.P., S.J., N.E.D., and J.-B.L.; Funding Acquisition, N.E.D. and J.-B.L.; Resources, S.J.; Supervision, N.E.D. and J.-B.L.

ACKNOWLEDGMENTS

We thank Drs Samir Hamdan and Antoine van Oijen for helpful discussions. This research was supported by Global Research Lab Program through the National Research Foundation (NRF) of Korea funded by the Ministry of Science and ICT (NRF-2017K1A1A2013241 to J.-B.L.), the University of Wollongong (collaborative travel grant to S.J.) and the Australian Research Council (DP150100956 to N.E.D.).

Received: January 6, 2017
Revised: August 9, 2017
Accepted: September 27, 2017
Published: November 2, 2017

REFERENCES

Bailey, S., Wing, R.A., and Steitz, T.A. (2006). The structure of *T. aquaticus* DNA polymerase III is distinct from eukaryotic replicative DNA polymerases. Cell *126*, 893–904.

Berezhna, S., and Gill, J. (2012). Single-molecule Förster resonance energy transfer reveals an innate fidelity checkpoint in DNA polymerase I. J. Am. Chem. Soc. *134*, 11261–11268.

Brenowitz, S., Kwack, S., Goodman, M.F., O'Donnell, M., and Echols, H. (1991). Specificity and enzymatic mechanism of the editing exonuclease of *Escherichia coli* DNA polymerase III. J. Biol. Chem. *266*, 7888–7892.

Capson, T.L., Peliska, J.A., Kaboord, B.F., Frey, M.W., Lively, C., Dahlberg, M., and Benkovic, S.J. (1992). Kinetic characterization of the polymerase and exonuclease activities of the gene 43 protein of bacteriophage T4. Biochemistry *31*, 10984–10994.

Carver, T.E., Jr., Hochstrasser, R.A., and Millar, D.P. (1994). Proofreading DNA: recognition of aberrant DNA termini by the Klenow fragment of DNA polymerase I. Proc. Natl. Acad. Sci. USA *91*, 10670–10674.

Cho, W.-K., Jergic, S., Kim, D., Dixon, N.E., and Lee, J.-B. (2014). Loading dynamics of a sliding DNA clamp. Angew. Chem. Int. Ed *53*, 6768–6771.

Christian, T.D., Romano, L.J., and Rueda, D. (2009). Single-molecule measurements of synthesis by DNA polymerase with base-pair resolution. Proc. Natl. Acad. Sci. USA *106*, 21109–21114.

Dalrymple, B.P., Kongsuwan, K., Wijffels, G., Dixon, N.E., and Jennings, P.A. (2001). A universal protein-protein interaction motif in the eubacterial DNA replication and repair systems. Proc. Natl. Acad. Sci. USA *98*, 11627–11632.

Dohrmann, P.R., and McHenry, C.S. (2005). A bipartite polymerase-processivity factor interaction: only the internal β binding site of the α subunit is required for processive replication by the DNA polymerase III holoenzyme. J. Mol. Biol. *350*, 228–239.

Donlin, M.J., Patel, S.S., and Johnson, K.A. (1991). Kinetic partitioning between the exonuclease and polymerase sites in DNA error correction. Biochemistry *30*, 538–546.

Echols, H., and Goodman, M.F. (1991). Fidelity mechanisms in DNA replication. Annu. Rev. Biochem. *60*, 477–511.

Fernandez-Leiro, R., Conrad, J., Scheres, S.H., and Lamers, M.H. (2015). Cryo-EM structures of the *E. coli* replicative DNA polymerase reveal its dynamic interactions with the DNA sliding clamp, exonuclease and τ. Elife *4*, e11134.

Fernandez-Leiro, R., Conrad, J., Yang, J.C., Freund, S.M., Scheres, S.H., and Lamers, M.H. (2017). Self-correcting mismatches during high-fidelity DNA replication. Nat. Struct. Mol. Biol. *24*, 140–143.

Fijalkowska, I.J., and Schaaper, R.M. (1996). Mutants in the Exo I motif of *Escherichia coli* dnaQ: defective proofreading and inviability due to error catastrophe. Proc. Natl. Acad. Sci. USA *93*, 2856–2861.

Franklin, M.C., Wang, J., and Steitz, T.A. (2001). Structure of the replicating complex of a Pol α family DNA polymerase. Cell *105*, 657–667.

Geertsema, H.J., Kulczyk, A.W., Richardson, C.C., and van Oijen, A.M. (2014). Single-molecule studies of polymerase dynamics and stoichiometry at the bacteriophage T7 replication machinery. Proc. Natl. Acad. Sci. USA *111*, 4073–4078.

Hamdan, S., Carr, P.D., Brown, S.E., Ollis, D.L., and Dixon, N.E. (2002a). Structural basis for proofreading during replication of the *Escherichia coli* chromosome. Structure *10*, 535–546.

Hamdan, S., Bulloch, E.M., Thompson, P.R., Beck, J.L., Yang, J.Y., Crowther, J.A., Lilley, P.E., Carr, P.D., Ollis, D.L., Brown, S.E., et al. (2002b). Hydrolysis of the 5′-*p*-nitrophenyl ester of TMP by the proofreading exonuclease (ε) subunit of *Escherichia coli* DNA polymerase III. Biochemistry *41*, 5266–5275.

Hamdan, S.M., Johnson, D.E., Tanner, N.A., Lee, J.B., Qimron, U., Tabor, S., van Oijen, A.M., and Richardson, C.C. (2007). Dynamic DNA helicase-DNA polymerase interactions assure processive replication fork movement. Mol. Cell *27*, 539–549.

Hwang, H., Kim, H., and Myong, S. (2011). Protein induced fluorescence enhancement as a single molecule assay with short distance sensitivity. Proc. Natl. Acad. Sci. USA *108*, 7414–7418.

Ibarra, B., Chemla, Y.R., Plyasunov, S., Smith, S.B., Lazaro, J.M., Salas, M., and Bustamante, C. (2009). Proofreading dynamics of a processive DNA polymerase. EMBO J. *28*, 2794–2802.

Jergic, S., Horan, N.P., Elshenawy, M.M., Mason, C.E., Urathamakul, T., Ozawa, K., Robinson, A., Goudsmits, J.M.H., Wang, Y., Pan, X., et al. (2013). A direct proofreader-clamp interaction stabilizes the Pol III replicase in the polymerization mode. EMBO J. *32*, 1322–1333.

Johansson, E., and Dixon, N. (2013). Replicative DNA polymerases. Cold Spring Harb. Perspect. Biol. *5*, a012799.

Johnson, D.E., Takahashi, M., Hamdan, S.M., Lee, S.J., and Richardson, C.C. (2007). Exchange of DNA polymerases at the replication fork of bacteriophage T7. Proc. Natl. Acad. Sci. USA *104*, 5312–5317.

Kalafut, B., and Visscher, K. (2008). An objective, model-independent method for detection of non-uniform steps in noisy signals. Comput. Phys. Commun. *179*, 716–723.

Kath, J.E., Jergic, S., Heltzel, J.M.H., Jacob, D.T., Dixon, N.E., Sutton, M.D., Walker, G.C., and Loparo, J.J. (2014). Polymerase exchange on single DNA molecules reveals processivity clamp control of translesion synthesis. Proc. Natl. Acad. Sci. USA *111*, 7647–7652.

Kong, X.-P., Onrust, R., O'Donnell, M., and Kuriyan, J. (1992). Three-dimensional structure of the β subunit of *E. coli* DNA polymerase III holoenzyme: a sliding DNA clamp. Cell *69*, 425–437.

Kunkel, T.A. (2004). DNA replication fidelity. J. Biol. Chem. *279*, 16895–16898.

Lamers, M.H., Georgescu, R.E., Lee, S.-G., O'Donnell, M., and Kuriyan, J. (2006). Crystal structure of the catalytic α subunit of *E. coli* replicative DNA polymerase III. Cell *126*, 881–892.

Lamichhane, R., Berezhna, S.Y., Gill, J.P., van der Schans, E., and Millar, D.P. (2013). Dynamics of site switching in DNA polymerase. J. Am. Chem. Soc. *135*, 4735–4742.

Lee, J.-B., Hite, R.K., Hamdan, S.M., Xie, X.S., Richardson, C.C., and van Oijen, A.M. (2006). DNA primase acts as a molecular brake in DNA replication. Nature *439*, 621–624.

Lehtinen, D.A., and Perrino, F.W. (2004). Dysfunctional proofreading in the *Escherichia coli* DNA polymerase III core. Biochem. J. *384*, 337–348.

Lewis, J.S., Spenkelink, L.M., Jergic, S., Wood, E.A., Monachino, E., Horan, N.P., Duderstadt, K.E., Cox, M.M., Robinson, A., Dixon, N.E., and van Oijen, A.M. (2017). Single-molecule visualization of fast polymerase turnover in the bacterial replisome. Elife *6*, e23932.

McHenry, C.S. (2011). DNA replicases from a bacterial perspective. Annu. Rev. Biochem. *80*, 403–436.

Miller, H., and Perrino, F.W. (1996). Kinetic mechanism of the 3′→5′ proofreading exonuclease of DNA polymerase III. Analysis by steady state and pre-steady state methods. Biochemistry *35*, 12919–12925.

Oakley, A.J., Prosselkov, P., Wijffels, G., and Beck, J.L. (2003). Flexibility revealed by the 1.85 Å crystal structure of the β sliding-clamp subunit of *Escherichia coli* DNA polymerase III. Acta Crystallogr. D Biol. Crystallogr. *59*, 1192–1199.

Ozawa, K., Horan, N.P., Robinson, A., Yagi, H., Hill, F.R., Jergic, S., Xu, Z.-Q., Loscha, K.V., Li, N., Tehei, M., et al. (2013). Proofreading exonuclease on a tether: the complex between the *E. coli* DNA polymerase III subunits α, ε, θ and β reveals a highly flexible arrangement of the proofreading domain. Nucleic Acids Res. *41*, 5354–5367.

Ozawa, K., Jergic, S., Crowther, J.A., Thompson, P.R., Wijffels, G., Otting, G., and Dixon, N.E. (2005). Cell-free protein synthesis in an autoinduction system for NMR studies of protein-protein interactions. J. Biomol. NMR *32*, 235–241.

Park, J., Jeon, Y., In, D., Fishel, R., Ban, C., and Lee, J.-B. (2010). Single-molecule analysis reveals the kinetics and physiological relevance of MutL-ssDNA binding. PLoS One *5*, e15496.

Park, M.S., and O'Donnell, M. (2009). The clamp loader assembles the β clamp onto either a 3′ or 5′ primer terminus. The underlying basis favoring 3′ loading. J. Biol. Chem. *284*, 31473–31483.

Reems, J.A., Griep, M.A., and McHenry, C.S. (1991). Proofreading activity of DNA polymerase III responds like elongation activity to auxiliary subunits. J. Biol. Chem. *266*, 4878–4882.

Rock, J.M., Lang, U.F., Chase, M.R., Ford, C.B., Gerrick, E.R., Gawande, R., Coscolla, M., Gagneux, S., Fortune, S.M., and Lamers, M.H. (2015). DNA replication fidelity in *Mycobacterium tuberculosis* is mediated by an ancestral prokaryotic proofreader. Nat. Genet. *47*, 677–681.

Santoso, Y., Joyce, C.M., Potapova, O., Le Reste, L., Hohlbein, J., Torella, J.P., Grindley, N.D.F., and Kapanidis, A.N. (2010). Conformational transitions in DNA polymerase I revealed by single-molecule FRET. Proc. Natl. Acad. Sci. USA *107*, 715–720.

Scheuermann, R.H., and Echols, H. (1984). A separate editing exonuclease for DNA replication: the ε subunit of *Escherichia coli* DNA polymerase III holoenzyme. Proc. Natl. Acad. Sci. USA *81*, 7747–7751.

Shamoo, Y., and Steitz, T.A. (1999). Building a replisome from interacting pieces: sliding clamp complexed to a peptide from DNA polymerase and a polymerase editing complex. Cell *99*, 155–166.

Steitz, T.A., Beese, L., Freemont, P.S., Friedman, J.M., and Sanderson, M.R. (1987). Structural studies of Klenow fragment: an enzyme with two active sites. Cold Spring Harb. Symp. Quant. Biol. *52*, 465–471.

Sutton, M.D. (2010). Coordinating DNA polymerase traffic during high and low fidelity synthesis. Biochim. Biophys. Acta *1804*, 1167–1179.

Tanner, N.A., Hamdan, S.M., Jergic, S., Loscha, K.V., Schaeffer, P.M., Dixon, N.E., and van Oijen, A.M. (2008). Single-molecule studies of fork dynamics in *Escherichia coli* DNA replication. Nat. Struct. Mol. Biol. *15*, 170–176.

Toste Rêgo, A., Holding, A.N., Kent, H., and Lamers, M.H. (2013). Architecture of the Pol III-clamp-exonuclease complex reveals key roles of the exonuclease subunit in processive DNA synthesis and repair. EMBO J. *32*, 1334–1343.

van Oijen, A.M., Blainey, P.C., Crampton, D.J., Richardson, C.C., Ellenberger, T., and Xie, X.S. (2003). Single-molecule kinetics of λ exonuclease reveal base dependence and dynamic disorder. Science *301*, 1235–1238.

Vallotton, P., and Olivier, S. (2013). Tri-track: free software for large-scale particle tracking. Microsc. Microanal. *19*, 451–460.

Whatley, Z., and Kreuzer, K.N. (2015). Mutations that separate the functions of the proofreading subunit of the *Escherichia coli* replicase. G3 (Bethesda) *5*, 1301–1311.

Wijffels, G., Dalrymple, B.P., Prosselkov, P., Kongsuwan, K., Epa, V.C., Lilley, P.E., Jergic, S., Buchardt, J., Brown, S.E., Alewood, P.F., et al. (2004). Inhibition of protein interactions with the β_2 sliding clamp of *Escherichia coli* DNA polymerase III by peptides from β_2-binding proteins. Biochemistry *43*, 5661–5671.

Williams, N.K., Prosselkov, P., Liepinsh, E., Line, I., Sharipo, A., Littler, D.R., Curmi, P.M.G., Otting, G., and Dixon, N.E. (2002). *In vivo* protein cyclization promoted by a circularly permuted *Synechocystis* sp. PCC6803 DnaB mini-intein. J. Biol. Chem. *277*, 7790–7798.

Wing, R.A., Bailey, S., and Steitz, T.A. (2008). Insights into the replisome from the structure of a ternary complex of the DNA polymerase III α-subunit. J. Mol. Biol. *382*, 859–869.

Yin, Z., Kelso, M.J., Beck, J.L., and Oakley, A.J. (2013). Structural and thermodynamic dissection of linear motif recognition by the *E. coli* sliding clamp. J. Med. Chem. *56*, 8665–8673.

STAR★METHODS

KEY RESOURCES TABLE

REAGENT or RESOURCE	SOURCE	IDENTIFIER
Antibodies		
Anti-digoxigenin, Fab fragments (from sheep)	Roche	11214667001; RRID: AB_514494
Anti-digoxigenin (from sheep)	Roche	11333089001; RRID: AB_514496
Bacterial and Virus Strains		
Escherichia coli BL21(λDE3)*recA*	Williams et al., 2002	N/A
Chemicals, Peptides, and Recombinant Proteins		
*Kas*I	New England Biolabs	R0544S
*Nb.Bbv*CI	New England Biolabs	R0632S
SYBR Gold	Life Technologies	S11494
Cesium chloride (CsCl)	Sigma	C4036
Ethidium bromide (EtBr)	Sigma	E1510-10ML
GeneRuler DNA Ladder mix, ready-to-use	Thermo Fisher Scientific	SM0331
T4 DNA ligase	Roche	10481220001
Cy3/Cy5 NHS Ester	GE Healthcare	PA13101 / PA15601
Dynabeads M-280 Tosylactivated	Life Technologies	14203
Biotin-PEG-SVA, MW5000	Laysan Bio	Biotin-PEG-SVA-5000-100mg
mPEG-succinimidyl valerate, MW5000	Laysan Bio	MPEG-SVA-5000-5g
Neutravidin protein	ThermoFisher	31000
E. coli DNA Pol III HE subunits α, δ and δ′	Wijffels et al., 2004	N/A
E. coli DNA Pol III HE subunit γ	Ozawa et al., 2005	N/A
E. coli DNA Pol III HE sliding clamp β_2	Oakley et al., 2003	N/A
E. coli DNA Pol III HE subunits ε and θ	Hamdan et al., 2002b	N/A
Subunit ε variants: ε_L, ε_Q and $\varepsilon_{D12A,E14A}$ (ε_{DEAD})	Jergic et al., 2013	N/A
Pol III core assemblies: $\alpha\varepsilon\theta$, $\alpha\varepsilon_L\theta$, $\alpha\varepsilon_Q\theta$ and $\alpha\varepsilon_{DEAD}\theta$	Jergic et al., 2013 Tanner et al., 2008	N/A
Minimal clamp loader subassembly: $\gamma_3\delta\delta'$	Jergic et al., 2013	N/A
Cy5 conjugated β_2 sliding clamp	Cho et al., 2014	N/A
Oligonucleotides		
Oligos for constructing 45.7 kb DNA, see Method Details	Integrated DNA Technology	N/A (custom order)
Oligos for constructing short DNAs, see Method Details	Integrated DNA Technology / Bioneer	N/A (custom order)
Recombinant DNA		
λ phage DNA	New England Biolabs	N3011S
p1644 plasmid for preparation of nicked DNA	This work	N/A
Software and Algorithms		
OriginPro 8	OriginLabs	N/A
Excel	Microsoft	N/A
Diatrack 3.0	Vallotton and Olivier, 2013	http://www.diatrack.org
Matlab R2013b	Mathworks	N/A
IDL 6.4	Exelis Visual Information Solutions	N/A
Custom IDL scripts	Taekjip Ha (Johns Hopkins Univ.)	N/A
Custom Matlab scripts	This work	

CONTACT FOR REAGENT AND RESOURCE SHARING

The singly-nicked 7.3 kb DNA template for the ensemble assay was a kind gift from Dr. Yao Wang (University of Wollongong). Further information and requests for resources and reagents should be directed to and will be fulfilled by the Lead Contact, Jong-Bong Lee (jblee@postech.ac.kr).

EXPERIMENTAL MODEL AND SUBJECT DETAILS

Cell Lines and Culture Conditions

All proteins and plasmids used for *in vitro* studies were purified from *Escherichia coli* K-12 strain BL21(λDE3)*recA* (Williams et al., 2002) as described in the text/resource table.

METHOD DETAILS

Replication Proteins

Overexpression and purification of subunits and complexes constituting Pol III holoenzyme have been described as follows: α, δ and δ′ (Wijffels et al., 2004), γ (Ozawa et al., 2005), β_2 (Oakley et al., 2003), θ (Hamdan et al., 2002b). The ε subunit and its variants ε_L, ε_Q and $\varepsilon_{D12A,E14A}$ (ε_{DEAD}) were as described (Hamdan et al., 2002b; Jergic et al., 2013). Pol III core assemblies, αεθ, $\alpha\varepsilon_L\theta$, $\alpha\varepsilon_Q\theta$ and $\alpha\varepsilon_{DEAD}\theta$, and the γ-clamp loader ($\gamma_3\delta\delta'$) complex were assembled from purified subunits (Tanner et al., 2008; Jergic et al., 2013). Cy5 conjugation to Cys333 of one subunit of β_2 using the cysteine-maleimide chemistry has also been described (Cho et al., 2014).

45.7 kb DNA for Flow-Stretching Assay

To construct the 45.7 kb DNA with 3′-biotin and 5′-digoxigenin (dig) ends on the same strand, λ phage DNA (New England Biolabs, USA) was cleaved with restriction endonuclease *KasI*, generating 45.7-kb and 2.8-kb fragments. The 3′-biotin (94 nt), 5′-dig (57 nt) and linker (19 nt) oligonucleotides were added and annealed after heating at 65°C for 5 min and slowly cooling to room temperature before ligation using T4 DNA ligase (Roche, USA) with 1 mM ATP for 16 h at 4°C.

Sequences of oligonucleotides used to construct templates for flow-stretching experiments (dT_{43} and p- indicate 43 nt long poly-thymidine and 5′-phosphorylation, respectively) were:

3′-biotin: 5′-p-AGG TCG CCG CCC AGT TAC AGA TTT ATG GTG ACG ATA CAA ACT ATA GAG TGA dT_{43}-/biotin/;

5′-dig: 5′-/dig/-GTA TCA TGA TTG TAG GTA CAC GTC AGC GAC AAG AGG CAG ACA TGA TGA ATT CTA ATG;

Linker: 5′-p-GCG CCA TTA GAA TTC ATC A.

Short DNAs for FRET and smPIFE Assays

The gapped duplex DNA was constructed after annealing PAGE- or HPLC-purified oligonucleotides (IDT, USA or Bioneer, Korea). Before annealing, Cy3 or Cy5 NHS-ester dyes (GE Healthcare, USA) were conjugated to the oligonucleotides that contain Amino Modifier C6 dT linker (C6dT). A total of 2 μl of oligos (1 mM, dissolved in deionized water) were mixed with 2 μl of Cy3- or Cy5-NHS (20 mM, dissolved in DMSO) in 10 μl of 0.1 M sodium tetraborate (pH 8.5). After incubating overnight, excess dyes were removed through ethanol precipitation. The gapped duplex DNAs with Cy3 alone (Figures 4A, 5E, and 5F) or both Cy3 and Cy5 (Figure 5A) were generated by mixing: Long-85nt, Biotin-Cy3-A, and Dig-30nt (for Figures 4A and 5E); Long-Cy5-85nt, Biotin-Cy3-T, and Dig-30nt (for Figure 5A); or Long-85nt, Biotin-Cy3-mismatch, and Dig-30nt (for Figure 5F) at a 1:1.2:1.4 molar ratio in annealing buffer (10 mM Tris.HCl at pH 8.0, 100 mM NaCl, 1 mM EDTA), incubation at 90°C for 5 min, then slow cooling to room temperature (> 3 h).

Sequences of oligonucleotides used in smFRET and smPIFE experiments:

Long-Cy5-85nt: 5′-ATG CGT ATC ATG ATT GTA GGT ACA CGT CAG AAG CCA GTC GCA CAG C/C6dT-Cy5/C CAC AGC ACG CGC ACA GAC AGC ACT GGA GTC CGT AGA A;

Biotin-Cy3-T: 5′-/biotin/-TTC TAC GGA CTC CAG /C6dT-Cy3/GC TGT CTG TGC GCG TGC TGT GGA GCT G;

Long-85nt: 5′-ATG CGT ATC ATG ATT GTA GGT ACA CGT CAG AAG CCA GTC ACA CAG CAC CAC AGC ACG CGC ACA GAC AGC ACT GGA GTC CGT AGA A;

Biotin-Cy3-A: 5′-/biotin/-TTC TAC GGA CTC CAG /C6dT-Cy3/GC TGT CTG TGC GCG TGC TGT GGT GCT G

Biotin-Cy3-mismatch: 5′-/biotin/-TTC TAC GGA CTC CAG /C6dT-Cy3/GC TGT CTG TGC GCG TGC TGT GGT AAA A;

Dig-30nt: CTG ACG TGT ACC TAC AAT CAT GAT ACG CAT-/dig/-3′.

2.8 μm Super-Paramagnetic Beads

Tosylactivated beads (Life Technologies, M-280, 2.8μm) were functionalized with antidigoxigenin (anti-dig) Fab fragments (Roche). A re-suspended bead stock (165 μl) was transferred to a 1.7 ml microtube, which is placed on a magnet (Dynal MPC). When the liquid became transparent after the beads were attracted to the tube surface due to the magnet, the supernatant was carefully removed and replaced by 1 ml of Buffer B1 (0.1 M H_3BO_3, pH 9.5 in deionized water). The solution was mixed by vortexing, and the supernatant was removed once again by the same procedure. Buffer B1 (50 μl) and 100 μl of anti-digoxigenin Fab (1 mg/ml) were added to the beads, and then mixed gently by tapping. Then 100 μl of Buffer B2 (3 M $(NH_4)_2SO_4$ dissolved in Buffer B1 or 0.1 M Na-phosphate buffer that

contains 0.02 M of NaH_2PO_4 and 0.08 M of Na_2HPO_4) were added, followed by a gentle tapping. The solution was incubated for 12–17 h at 37°C with slow rotation to prevent the aggregation of the beads. The supernatant was removed using the magnet, and incubated another 1 h at 37°C after the addition of 1 ml of Buffer B3 [1x PBS pH 7.4 with 0.5% (w/v) BSA]. The supernatant was removed, and 1 ml of Buffer B4 [1x PBS pH 7.4 with 0.1% (w/v) BSA] was added, followed by a gentle tapping for 2 min. After repeating this step one more time, 400 μl of fresh Buffer B4 was added for storage at 4°C.

Flow-Stretching Assays

The 45.7-kb DNA was immobilized on a PEG/PEG-biotin (Laysan Bio, USA) surface using the biotin–neutravidin interaction, and a 2.8 μm anti-dig antibody-coated superparamagnetic bead (Invitrogen, USA) was attached to the 5′-dig end of the DNA in 20 mM Tris-HCl (pH 8), 2 mM EDTA, 50 mM NaCl, 0.1 mg ml^{-1} BSA and 0.025% Tween 20. Replication proteins and dNTPs (as indicated) were infused in 25 mM Tris-HCl (pH 7.5), 100 mM NaCl, 8 mM $MgCl_2$, 10 mM dithiothreitol, and 1 mM ATP. The beads were imaged using an optical microscope with a 10x objective (NA = 0.4, Olympus) and data recorded using a CCD (QImaging, RETIGA 2000R) camera at a 500 ms sampling rate using MetaVue (Molecular Devices) software.

Ensemble DNA Replication Assays

The 7.3-kb colE1 plasmid p1644, which contains a single recognition site for the nicking endonuclease *Nb.BbvCI* was extracted from a BL21(λDE3)*recA* culture using a Maxiprep kit (Qiagen) and further purified by cesium-cloride (CsCl) gradient centrifugation in the presence of ethidium bromide (EtBr). Recovered supercoiled plasmid was nicked using *Nb.BbvCI*, then subjected to another round of CsCl/EtBr gradient centrifugation. The upper of the two bands was finally isolated, yielding purified singly-nicked plasmid DNA.

The standard exonuclease assay contained 50 nM $\gamma_3\delta\delta'$ clamp loader complex, 200 nM β_2, 100 nM of the indicated cores ($\alpha\varepsilon_L\theta$, $\alpha\varepsilon\theta$ or $\alpha\varepsilon_Q\theta$), 1 mM ATP and 3.1 nM nicked (7.3 kb) DNA template in a replication buffer comprised of 20 mM Tris.HCl at pH 7.6, 10 mM $MgCl_2$ and 10 mM dithiothreitol, in a final volume of 13 μl. All components were mixed on ice, reactions were then initiated by quick transfer to a 30°C water bath and quenched after denoted times by the addition of a 12 μl quenching buffer containing 200 mM EDTA, 2% (w/v) SDS, 0.08% (w/v) bromophenol blue, 0.08% (w/v) xylene cyanol and 10% (v/v) glycerol. Final mixtures were treated for 5 min at 42°C and loaded onto a 0.66% agarose gel in 2x TAE buffer together with a sample(s) of GeneRuler DNA Ladder mix (Thermo Fisher Scientific). Products were separated by electrophoresis at 70 V for 150 min. Resolved gel products were stained for 1.5 h in SYBR Gold (Life Technologies) and DNA bands visualized under 302-nm UV light using a Gel Doc™ XR+ system (Bio-Rad, Hercules, CA).

Single-Molecule Fluorescence Imaging

Approximately 10 pM of the duplex DNA was incubated on the PEG/PEG-biotin quartz surface for 5 min and the free end was blocked with 50 nM anti-dig antibody (Roche) for 10 min. Approximately 30 nM of β_2 clamp, 15 nM of γ clamp loader ($\gamma_3\delta\delta'$) and 1 mM ATP were incubated for 2 min to load β_2 onto immobilized DNA. Subsequently, the reaction buffer (500 μl) containing Pol III cores at the indicated concentrations were injected into the reaction chamber (6 μl), displacing excess γ clamp loader and β_2 in solution. The reaction buffers were identical to those described in the flow-stretching assay, except for the addition of an oxygen scavenging system (1–2 mM Trolox, 0.8% (w/v) D-glucose, 165 U ml^{-1} glucose oxidase, 2,170 U ml^{-1} catalase). Emission signals from both a Cy3 donor excited with a 532 nm DPSS laser (Cobalt, 100 mW) and an Cy5 acceptor were collected in a wide-field prism-type total internal reflection fluorescence microscopy (TIRFM) setup using an inverted optical microscope (Olympus, IX-71) with a 60x water-immersion objective (NA = 1.2, Olympus). A neutral density (ND) filter (Thorlabs, NDC-25C-4M) was used to adjust the incident intensity (10 mW). The FRET signals were recorded using an EM-CCD camera (Hamamatsu, C9100-13, Japan) and MetaMorph software (Molecular Devices, USA) at a 30-ms time resolution. For PIFE experiments, we measured Cy3 signals emitted from the gapped duplex DNA with Cy3 alone for 3′ gap DNA (Figure 5E) or Cy3 and mismatched nucleotides for 3′ flap DNA (Figure 5F) using methods identical to the FRET experiments.

QUANTIFICATION AND STATISTICAL ANALYSIS

Data fitting and statistical analyses were done using OriginPro8 (OriginLabs, USA) and Excel (Microsoft, USA). For sample comparisons, Student's t-test with two samples was performed for sample comparison assuming equal or unequal variances. Each pair of variances was determined to be equal or not through F-test. All tests were executed in Excel. Details of statistical values are reported in each Figure Legend.

Flow-Stretching Assays

The position of the bead was determined and tracked using 2D Gaussian fitting with 10-nm accuracy. The collected data were analyzed using DiaTrack3.0 software (Semasopht, Austrailia), Matlab R2013b (Mathworks Inc., USA), and OriginPro8 (OriginLab, USA). We converted the position of the bead measured in nm to the number of nucleotides excised. To determine the conversion factor of 3.2 nt nm^{-1}, we first measured the difference of the bead positions between 45.7 kb ds and ssDNA at an applied drag force of 2.5 pN and divided the total number of nucleotides by the difference in extension between ds and ssDNA. The net drag force acting on the bead was calculated using a vector sum of the magnetic force (*z*-axis) perpendicular to the sample chamber surface and the hydrodynamic force (*x*-axis), determined after measuring the mean-square displacement of a bead in the transverse direction of each

force (Park et al., 2010). We measured the full width half maximum (FWHM) of the Brownian fluctuations of DNA-attached beads in the flow direction in the absence of proteins. The curve of the FWHMs (n = 140) was a normal distribution from which we obtained an average of the FWHM as 38 ± 5 nm (mean ± SD) at a frame rate of 2 Hz and 2.5 pN. The spatial resolution corresponds to 38 nm x 3.2 nt nm^{-1} = 121.6 nt when dsDNA is converted into ssDNA. The exonuclease rates were determined as a linear fit to the middle 70% of individual slopes in the time trajectory.

Single-Molecule Fluorescence Imaging

We used a mixture of double- and single-Cy5 labeled β_2 for the single-molecule FRET experiments. The ratio of single- to double-Cy5 labeled β_2 was determined to be 9:1 as determined by double-Cy5 labeled β_2 showing two photobleaching steps in the single-molecule intensity trajectory. We rarely observed the two-step photobleaching in our experiments. We excluded the FRET signals of double-labeled β_2 from the data analysis by recording photobleaching steps in all experiments, so the single-molecule data we present were analyzed exclusively from single-Cy5 labeled β_2. The time course of individual FRET efficiency traces was obtained using IDL (Exelis Inc., USA) and Matlab R2013b scripts considering Cy3 leakage to the Cy5 channel and a correction factor (Park et al., 2010).

DATA AND SOFTWARE AVAILABILITY

Custom IDL and Matlab scripts were used to analyze fluorescence imaging data. Since the original IDL scripts were kindly provided by Dr. Taekjip Ha's laboratory (Johns Hopkins Univ., Baltimore), it is not appropriate for us to distribute them. The Matlab scripts are available upon request to J.-B. Lee (jblee@postech.ac.kr).